UDC: 517.9:519.6

Liubov ZHURAVCHAK[1], Nataliya ZABRODSKA[2]

[1] Lviv Polytechnic National University, 12, S. Bandery str., Lviv, 79013, Ukraine, tel. +38(032)2582578, e-mail: liubov.m.zhuravchak@lpnu.ua, https://orcid.org/0000-0002-1444-5882
[2] Carpathian branch of S. Subbotin Institute of Geophysics of National Academy of Sciences of Ukraine, 3-b, Naukova str., Lviv, 79060, Ukraine, tel. +38(032)2648563, e-mail: nataliya.zabrodska@gmail.com, https://orcid.org/0009-0001-8850-6721

https://doi.org/10.23939/jgd2025.02.057

CONSIDERATION OF INDUCED POLARIZATION EFFECTS IN SOLVING INVERSE PROBLEMS OF GEOELECTRICAL SOUNDING

The paper aims to develop an algorithm for identifying the physical (polarizability and resistivity) and geometric (center of mass, orientation, and dimensions) characteristics of local heterogeneities. This is achieved by analyzing induced polarization (IP) potential field data measured at the boundary of the object, using the indirect near-boundary element method. Methodology. A piecewise homogeneous half-plane was chosen as a model of the Earth's crust, where the components are in non-ideal contact. An efficient combination of the indirect near-boundary element method with a cascade iterative algorithm for parameter identification was developed to solve the inverse two-dimensional problem of the IP potential field theory. At each step of the algorithm, a series of direct problems was solved, in which the Laplace equations were transformed into integral representations. This transformation utilized the Green's function for a half-plane, which automatically satisfies the boundary condition and eliminates the need for boundary discretization. Additionally, a fundamental solution for the inclusion was applied. The conditions of non-ideal contact were satisfied in the collocation sense at the midpoints of each boundary element. This made it possible to determine the intensities of the unknown sources introduced into the near-boundary elements and approximated by constants. The medium and the inclusion were then treated as independent regions, and the desired IP field potential and flow across their boundaries were calculated. Results. A computational experiment was conducted for the problem of geoelectrical sounding using a constant artificial field (electrical profiling method). Initial estimates of the physical and geometric characteristics of the inclusion were obtained based on the behavior of apparent resistivity and apparent polarizability. Through two cascades of iterations, the location and approximate dimensions of the inclusion were first refined, followed by adjustments to its shape and spatial orientation. A necessary condition for successful identification was the presence of a boundary segment with an excess of boundary conditions, which enabled the minimization of the selected functional on that segment. Originality. The problem of geoelectrical sounding by direct current in piecewise homogeneous polarized media was reduced, via mathematical modeling, to a potential theory problem with non-ideal contact conditions at the interfaces between different media. Practical significance. An efficient computational approach was developed for solving the inverse problem of geoelectrical sounding using direct current. It considers the effect of induced polarization, including surface, volume, and mixed polarization. Computational efficiency was achieved through a two-stage cascade- iterative algorithm that refined initial approximations and eliminated parameters with negligible impact on the results.

Keywords: mathematical modeling, induced polarization, direct problem, inverse problem, indirect near-boundary element method, piecewise homogeneous polarized medium, electrical profiling.

Introduction

Mathematical models of the induced polarization (IP) effect enable the study of potential field distributions in heterogeneous media, which is particularly important in regions with tectonic activity. Based on the calculated apparent resistivity and polarizability, such models allow the identification of fluid-saturated zones, faults, boundaries of tectonic blocks, and metasomatic zones – processes directly related to geodynamic changes in the lithosphere. These models enable interpreting experimental data while accounting for the complex geometry of inclusions and variations in physical parameters, which is essential for constructing reliable geoelectrical cross-sections. They also support both qualitative and quantitative analysis of geoelectrical properties for describing complex geological processes in the Earth's interior. Numerical modeling enhances theinterpretation of data obtained from the induced polarization method. It is also a powerful tool for investigating the Earth's deep structure and the mechanisms of tectonic activity. Additionally, it plays a crucial role

monitoring the development of fault zones, an essential aspect of geodynamic analysis.

A rigorous physico-mathematical model of a heterogeneous conducting medium proposed by [Zhdanov, 2008] is based on the effective medium approach. The generalization of the classical theory of effective media (TEM) consists of two main components: the introduction of an effective conductivity model for heterogeneous, multiphase rocks with inclusions of arbitrary shape, conductivity, and polarizability using quasi-linear approximation principles within the TEM formalism, and the development of a generalized effective-medium theory that incorporates induced polarization (GEMTIP). This model accounts for both electromagnetic induction (EMI) and induced polarization (IP) effects associated with the relaxation of polarized charges in rocks. The geoelectrical parameters of this model are determined by the composite medium's internal petrophysical and geometrical characteristics, such as mineralization and/or fluid content in the rocks, matrix composition, porosity, anisotropy, and formation polarizability. In a simplified version involving spherical inclusions, GEMTIP is consistent with the empirical Cole–Cole model and the classical IP model proposed by Wait.

In [Ye et al., 2014], an adaptive finite element method for 2.5D modeling of the IP effect is proposed, which uses an irregular grid with triangular elements and allows for describing the of complex geological structure geometry, particularly inclined layers and uneven terrain, with local refinements. In [Hongzhu, Zhdanov, 2017], an approach to modeling the IP response in 3D dispersed conducting media is proposed, using the finite element method in the time domain, an unstructured tetrahedral grid, stable time discretization, and the Cole-Cole model with an adaptive Padé expansion to accurately account for conductivity dispersion.

In the article [Yanju et al., 2018], a new method for numerical simulation of electromagnetic signals is presented. This method, based on the finite difference approach, in the time domain is specifically designed for 3D polarization media with consideration of IP effects. The approach utilizesthe Cole-Cole model and addresses challenges relatedfractional derivatives. Numerical experiments have shown that the medium's size, charge and frequency dependence significantly affect the detection of polarization bodies, and small objects remain difficult to register with modern methods.

In [Kamran, Hamidreza, 2019], the authors investigate the effectiveness of the IP method for modeling ore bodies and optimizing drilling operations using the example of the Madan Bozorg copper deposit in Abbasabad, Iran. They combined IP, electrical resistivity, and copper content data from drill holes to create two- and three-dimensional ore distribution models. Using geostatistical methods (cokriging) and artificial neural networks, they predicted the location of ore bodies in areas without drill data. The results showed a high agreement between the predicted and actual data, which allowed for reducing the number of required drill holes by approximately 45 % and optimizingtheir location. This study demonstrates the potential of the IP method as an effective tool for reducing costs and increasing accuracy in geological exploration.

In Saudi Arabia, the Glass Earth geophysical project [Alfouzan et al., 2020] was successfully implemented on m ore than 8,000 km² of previously unexplored territory to search for minerals, water, and geothermal resources. Aerogeophysics, spectral induced polarization, and GEMTIP inversion were used, which takes into account 3D electromagnetic (EM) effects. A method was developed that considers all three-dimensional EM effects when inverting IP data. [Yanju et al., 2020] presents a three-dimensional numerical simulation of the VP for the GREATEM system using the fictitious wave field method and the Colem-Kerr model. It allows for effective simulation of the VP in a polarized environment, reducing the calculation time by a factor of five compared to traditional methods. It has been shown that IP effects are better manifested in high-resistivity zones, and are practically not recorded in low-resistivity zones.

The article [Revil et al., 2021] investigates the application of the IP method to construct the temperature field inside shield volcanoes. The authors analyze the dependence of the electrical properties of volcanic rocks on t emperature and humidity using experimental data and numerical modeling. The results show that the IP method allows you to detect hot zones and thermal anomalies, which are important for geothermal monitoring and assessing the potential activity of volcanoes. In 2015, an induced polarization survey was conducted on the Kilauea volcano. Charge and conductivity tomograms were obtained using 64 electrodes and 6,210 measurements. A conductivity / polarization model was used to determine the temperature tomograms, which allows these parameters to be used as temperature sensors.

In [Caowei et al., 2022], a numerical simulation was conducted to study the relationship between mineralized structures and IP properties of marine polymetallic sulfide rocks. The effect of sulfide content on charge and electrical conductivity was investigated, which is relevant for electrical studies of marine deposits. The simulation shows how the mineralization structure affects IP properties in seafloor sulfide rocks. The article [Bérubé, Charles, Bérubé, Pierre, 2022] presents a new approach to IP modeling

in the time domain using variational autoencoders (VAE). The model is trained on more than 1.6 million IP decay curves collected in Canada, the United States, and Kazakhstan. The approach allows for synthetic data generation, Bayesian noise cleaning, signal-to-noise estimation, and outlier detection without the need for manual tuning or empirical models.

In [Satoshi, 2023], a method for modeling the polarization of metal grains in a 3D environment using OpenFOAM was developed. The paper studied the influence of the shape, size of the channels, orientation, and interaction of the grains on the potential distribution. This allows for a better understanding of the mechanisms of IP in complex conditions. The results will help improve models, interpretation, and laboratory experiments. [Davies, et al., 2023] presents a Bayesian approach to detecting IP effects in airborne electromagnetic (AEM) data. The authors developed an approach that combines a split-layer model with a Monte Carlo algorithm and reversible jumps (Reversible Jump Sequential Monte Carlo, RJSMC). It allows for simultaneous estimation of the parameters and model structure, taking into account the uncertainty in the number of layers in the geological environment. A statistical criterion is proposed for assessing IP detection based on the model posterior probabilities. The method was tested on large-scale AEM data, demonstrating its effectiveness in detecting IP effects that previously had no established methodology in aviation geophysics.

In the study [Zibulski, Klitzsch, 2023], the authors analyze the effect of grain internal surface roughness on spectral induced polarization (SIP) in laboratory measurements. Using models with smooth and rough surfaces, they simulate the SIP response, focusing on the polarization of the electric double layer around the particles. Roughness is modeled in two ways: by adding fractal structures to the surface and by generating random rough surfaces. The results show that surface roughness leads to changes in the frequency dependence and magnitude of polarization, which is important for interpreting SIP data in geophysical studies. The study emphasizes the importance of considering the microstructural features of rocks when analyzing SIP data, which can improve the accuracy of geophysical models and interpretations. A strong correlation is established between the strength of electric polarization and the internal surface of rocks. The effect of surface roughness on the SIP response was investigated, and two main effects were identified: relaxation frequency shift and secondary polarization formation.

[Cox et al., 2023] considers the physical and mathematical foundations of the method of aero-excited induced polarization. A method of joint inverse modeling is proposed to obtain electrical conductivity and parameters of the IP using the GEMTIP theory. The results of 3D modeling for the Echum area, Canada are presented. To model the IP in an anisotropic environment, the authors of [Jiaxuan, et al., 2024] used 2D Fourier transform and integration by shape functions. The method reduces computational costs, provides high accuracy and efficiency, and takes into account the anisotropy of polarization, which significantly affects the results of field measurements.

In [Pourhashemi, et al., 2024], the inversion of time-domain IP tomography is considered to determine the charge distribution in geomaterials. The technique allows for improving the characterization of near-surface structures, which is useful for mineral exploration, engineering, and environmental studies. The finite difference method is used to solve the Poisson equation, and the inversion algorithm is used to obtain resistivity and charge models of the near-surface layer.

The paper [Finden, et al., 2024] investigated the possibility of using IP in the transient electromagnetic reconnaissance method for detecting near-surface ice on Earth, Mars, and the Moon. Numerical simulations show that IP can detect ice, especially if it contains salts. [Bérubé, Gagnon, 2025] presented an approach to modeling anisotropic IP using a combination of neural networks and GEMTIP, which allows significant acceleration (up to 100,000 times) of calculations without significant loss of accuracy, which is promising for effective IP modeling in complex geological conditions for rapid calculation of depolarization tensors in anisotropic environments.

In [Fys, et al., 2023], the conventional approach to constructing a three-dimensional distribution of the Earth's masses involves using Stokes constants incrementally up to a certain order. Based on the mathematical modeling and the described algorithm, a three-dimensional model of the density distribution of subsoil masses in the middle of the Earth is obtained. It takes into account Stokes constants up to the eighth order inclusively and corresponds to the surface distribution of masses of the oceanic model of the Earth, its concise interpretation is also presented.

The article [Brusak et al., 2025] develops a method for detecting geodynamic anomalies in GNSS time series using machine learning algorithms. The method, which has been implemented in the Python environment, allows for the semi-automated analysis of large datasets.

Rocks capable of polarization are characterized by two parameters (resistivity ρ or electrical conductivity $\sigma = 1/\rho$ and polarizability η) or one $\rho^* = \rho(1-\eta)$ or $\sigma^* = \sigma\ (1-\eta)$, which is interpreted as the specific

resistivity or electrical conductivity of the polarized medium. The induced polarization method is based on measuring secondary electric fields of electrochemical and electrokinetic nature that arise in rocks when an electric current flows through them. It is one of the leading geophysical methods used to search and explore ore deposits. The IP method is used in both profiling and sounding modifications, using the same installations as in resistivity methods.

The resistivity and induced polarization methods are most often implemented together,if there is equipment for measuring non-stationary fields. Usually, anomalies of significantly increased values of apparent polarization η_a are observed over ore objects, in particular sulfide and graphitized ones. For a heterogeneous environment η_a, the spatial distribution of rock sections with different polarization depends on their specific electrical resistivity, the location of the feed and measuring electrodes, and the polarizing field's nature. By studying the spatial distribution of η_a, its dependence on the specified factors and taking into account the true polarization of the rocks that make up the area, it is possible, using geological data, to establish the features of the geoelectric section and on this basis to solve the problems of geological mapping and prospecting for mineral deposits.

The interpretation of the profiling results by the VP method is mainly qualitative. It comes down to selecting anomalies with increased apparent polarizability relative to background values. Quantitative interpretation is used for individual anomalies caused by local objects of simple shape. It is based on analytical solutions of the direct problem for bodies of simple geometric shape: a sphere, a cylinder, a vertical layer, etc. Analytical solutions to potential theory problems for piecewise homogeneous regions can be found by classical methods only for inclusions of a canonical or close-to-canonical shape. Consequently, there has been a growing reliance on numerical methods in mathematical modeling, especially for three-dimensional objects of arbitrary shapes. Recent years have seen an increase in the use of modern high-speed computers, particularly with accelerated modeling techniques such as GPU computing, adaptive meshes, hybrid methods, and machine learning algorithms for data interpretation [Zhuravchak, 2019; Zhuravchak, 2024].

Purpose

The paper aims to build an algorithm for recognizing physical (polarizability and resistivity) and geometric (center of mass, orientation, and size) characteristics of local inhomogeneity based on the field potential of induced polarization measured at the object's boundary.

Methodology

Problem formulation

Let us consider the problem of determining the physical (polarizability and electrical conductivity) and geometrical (center of mass, orientation, and dimensions) characteristics of a local inhomogeneity Ω_1 based on the pattern of the induced polarization (IP) potential field flow on the electrically insulated boundary $\Gamma = \{(x_1, x_2) : -\infty < x_1 < \infty,\ x_2 = 0\}$ of a half-plane. The half-plane occupies a domain $\Omega = \Omega_0 \cup \Omega_1 \cup \partial\Omega_1 = \mathbf{R}^{2-} = \{(x_1, x_2) : -\infty < x_1 < \infty, -\infty < x_2 < 0)$ in the Cartesian coordinate system (x_1, x_2), where $\partial\Omega_1$ denotes the interface between different media.

Two main types of polarization are observed in electronic conductors: surface and volume. Surface polarization is typical for large, solid ore bodies, where secondary charges accumulate on the surface under the influence of an external electric current. When the current is switched off, the accumulated energy dissipates (relaxes) over several seconds.

Volume polarization is characteristic for embedded ores not detected by other geophysical methods. The IP method is the main research method when searching for such objects. Non-ore rocks (sedimentary and igneous) are polarized much more weakly. In addition, the IP method is also used in hydrogeological geophysics to determine the groundwater level and identify various lithological rock complexes in the section due to the noticeable dependence of the polarization of sedimentary rocks on humidity, clay content, and porosity. Therefore, the main areas of application for the IP method include: mineral (especially ore) exploration, hydrogeology, and geological mapping. The increasing use of the IP method in petroleum exploration is also worth noting. Numerous field experiments have demonstrated that accumulations of pyrite inclusions often form above hydrocarbon reservoirs, creating favorable physical conditions for detecting and delineating oil and gas deposits.

We consider three possible types of polarization effects:

– surface polarization, resulting from the effect of a single conductive inclusion or a compact ore body embedded in a medium with ionic conductivity;

– volume polarization, arising from the cumulative effect of many conductive inclusions;

– mixed polarization, which combines aspects of both surface and volume mechanisms.

From a mathematical perspective, these cases can be modeled by imposing non-ideal contact conditions at the interface between different media:

surface polarization:

$$u_0(x)-u_1(x)=-\lambda\frac{\partial u_0(x)}{\partial \mathbf{n}(x)},$$

$$\sigma_0\frac{\partial u_0(x)}{\partial \mathbf{n}(x)}=\sigma_1\frac{\partial u_1(x)}{\partial \mathbf{n}(x)},\ x\in\partial\Omega_1, \qquad (1)$$

volume polarization:

$$u_0(x)=u_1(x),$$

$$\sigma_0^*\frac{\partial u_0(x)}{\partial \mathbf{n}(x)}=\sigma_1^*\frac{\partial u_1(x)}{\partial \mathbf{n}(x)},\ x\in\partial\Omega_1, \qquad (2)$$

mixed polarization:

$$u_0(x)-u_1(x)=-\lambda\frac{\partial u_0(x)}{\partial \mathbf{n}(x)},$$

$$\sigma_0^*\frac{\partial u_0(x)}{\partial \mathbf{n}(x)}=\sigma_1^*\frac{\partial u_1(x)}{\partial \mathbf{n}(x)},\ x\in\partial\Omega_1. \qquad (3)$$

Here λ_0 is a surface polarization coefficient on $\partial\Omega_1$, $\sigma_m^*=\sigma_m(1-\eta_m)$, σ_m is an electrical conductivity of W_m, m=0,1; η_m is a coefficient of induced polarizability of the medium in W_m, i.e. the ratio of the residual potential difference of the field caused by polarization, measured 0.5 s after the electric current in the power line is turned off, to the potential difference measured during the passage of the electric current before it is turned off; $\mathbf{n}(x)$ is the external uniquely defined unit normal to the boundary $\partial\Omega_0$ of the domain Ω_0.

The first of the equalities (2) is fulfilled only when there are no contact electromotive forces (EMF) at the interface. In the case of the latter, when crossing the boundary, a jump in the potential of the IP field will be observed, equal in magnitude to this contact EMF (the first ones of the equalities (1), (3)).

At the boundary G the potential field flow IP is zero everywhere, except for the section $\Gamma_j\subset\Gamma$ (not necessarily single-connected), in which the current sources are located:

$$-\sigma_0\frac{\partial u_0(x_1,0)}{\partial \mathbf{n}(x_1,0)}=j(x_1,0),\ (x_1,0)\in\Gamma_d, \qquad (4)$$

$$-\sigma_0^*\frac{\partial u_0(x_1,0)}{\partial \mathbf{n}(x_1,0)}=j(x_1,0),\qquad (x_1,0)\in\Gamma_d, \qquad (5)$$

where $j(x_1,0)\neq 0$ at $(x_1,0)\in\Gamma_j$, $j(x_1,0)=0$ at $(x_1,0)\notin\Gamma_j$. Note that in the case of surface polarization, we choose boundary condition (4), we choose boundary conditions (4) and (5) for volume and mixed polarization.

In addition, there is a region $\P W_b \grave{I} G$ where the potential value was additionally measured:

$$u_0(x_1,0)=u_b(x_1,0),\quad (x_1,0)\in\Gamma_b. \qquad (6)$$

Inside the half-plane, the potential of the IP field satisfies the equation:

$$P(u_m(x))=\sum_{i=1}^{2}\frac{\partial^2 u_m(x)}{\partial x_i^2}=0,\ x\in\Omega_m,\ m=0,1, \qquad (7)$$

where $x=(x_1,x_2)$ are the Cartesian coordinates.

As we can see, the introduction of a new characteristic of the environment model (polarizability) allows us to preserve the structure of the basic equations and simplify the solution of direct and inverse geoelectrical prospecting problems for models of polarizable objects.

Solving the direct problem of the theory of the potential field of the IP for the case of surface polarization

When solving a direct problem, we assume that all characteristics of local heterogeneity and the containing medium are known.

According to the basic principles of the indirect near-boundary element method [Zhuravchak, Zabrodska, 2010; Zhuravchak, Kruk, 2015], let us consider the set $\mathbf{R}^2(2)$ composed of two planes $\mathbf{R}_m^2$, which has the following properties:

$$\mathbf{R}_m^2\cap\mathbf{R}^2=\Omega_m\cup\partial\Omega_m,\ \mathbf{R}^2(2)\cap\mathbf{R}^2=\Omega\cup\Gamma,$$

$$\mathbf{R}_0^2\cap\mathbf{R}_1^2=\partial\Omega_1.$$

Contact boundary and external near-boundary areas

$$G_m=B_m\setminus\Omega_m,$$

where $B_m\subset\mathbf{R}_m^2$, $W_m \grave{I} B_m$, $\P W_m \c \P B_m=\AE$, are discretized into boundary G_v and near-boundary G_{mv} elements, respectively, so that each boundary element corresponds to two near-boundary elements:

$$G_{mv}\c\P W_1=G_v,\ G_{mv}\c G_{mq}=\AE,\ v\neq q,$$

$$v,q=\overline{1,V},\ \grave{E}_{v=1}^{V}G_{mv}=G_m.$$

We approximate the intensities of unknown fictitious sources introduced in the near-boundary elements by constants d_{mv}, considering that the sources are chosen on the boundary of the half-plane in the form of

$\psi(x_1,0)=-2j(x_1,0)/\sigma_0$ for volume and $\psi(x_1,0)=-2j(x_1,0)/\sigma_0^*$ for mixed polarization ensures the fulfillment of conditions (4), (5), and we pass from differential equations (7) to their integral representations, i.e., we write down the potentials $u_m(x,\sigma_m)$ of the IP field and their intensities

$$e_m(x,\sigma_m)=-\frac{\partial u_m(x,\sigma_m)}{\partial \mathbf{n}(x)}:$$

$$u_0(x,\sigma_0)=\sum_{v=1}^{V} d_{0v}\int_{G_{0v}} \mathbf{E}_{0h}(x,\xi,\sigma_0)dG_{0v}(\xi)+$$
$$+\int_{\Gamma_j} \mathbf{E}_{0h}(x,\xi,\sigma_0)\psi(\xi_1,0)d\Gamma_j(\xi)\,,\ x\in\Omega_0\cup\partial\Omega_0\,,$$
$$e_0(x,\sigma_0)=-\sum_{v=1}^{V} d_{0v}\int_{G_{0v}} \mathbf{F}_{0h}(x,\xi,\sigma_0)dG_{0v}(\xi)-$$
$$-\int_{\Gamma_j} \mathbf{F}_{0h}(x,\xi,\sigma_0)\psi(\xi_1,0)d\Gamma_j(\xi)\,, \qquad (8)$$
$$u_1(x,\sigma_1)=\sum_{v=1}^{V} d_{1v}\int_{G_{1v}} \mathbf{E}_1(x,\xi,\sigma_1)dG_{1v}(\xi)+C_1\,,$$
$$x\in\Omega_1\cup\partial\Omega_1\,,$$
$$e_1(x,\sigma_1)=-\sum_{v=1}^{V} d_{1v}\int_{G_{1v}} \mathbf{F}_1(x,\xi,\sigma_1)dG_{1v}(\xi)\,. \qquad (9)$$

Here $\mathbf{E}_{0h}(r,\mathsf{s}_0)=\mathbf{E}_0(r,\mathsf{s}_0)+\mathbf{E}_0(r',\mathsf{s}_0)$ is the Green function of the operator $P(u_0(x))$ for the half-plane, which automatically satisfies the boundary conditions (4), (5) at $j(x_1,0)=0$;

$$\mathbf{E}_m(r,\mathsf{s}_m)=\mathbf{E}_m(x,\mathsf{x},\mathsf{s}_m)=-\frac{1}{2\pi\mathsf{s}_m}\ln|r/r_0|$$

is the fundamental solution of the operators $P(u_m(x))$ for the plane;

$$\mathbf{F}_{0h}(r,\mathsf{s}_0)=\mathbf{F}_0(r,\mathsf{s}_0)+\mathbf{F}_0(r',\mathsf{s}_0),$$
$$\mathbf{F}_m(r,\mathsf{s}_m)=\mathbf{F}_m(x,\mathsf{x},\mathsf{s}_m)=\mathsf{s}_m^{-1}\sum_{i=1}^{2}\frac{n_i(x_i-\mathsf{x}_i)}{2\pi r^2},$$
$$\xi=(\xi_1,\xi_2)\in\mathbf{R}_m^2\,,$$

$\mathsf{x}_1,\mathsf{x}_2$ is a coordinate system that coincides with x_1,x_2,

$$r=\sqrt{(x_1-\mathsf{x}_1)^2+(x_2-\mathsf{x}_2)^2}\,,$$
$$r'=\sqrt{(x_1-\mathsf{x}_1)^2+(x_2+\mathsf{x}_2)^2}\,,$$

constant r_0 is used to improve the accuracy of calculations.

Here and further, we choose the values σ_0,σ_1 for surface polarization, and σ_0^*,σ_1^* for volume and mixed polarization. Note also that the current density, using (8) and (9), is found as

$$j_m(x,\sigma_m)=\sigma_m e_m(x,\sigma_m)\,.$$

We apply the collocation method to satisfy the contact conditions (1) in the middle of the boundary elements: in the points $x\in\Gamma_w$ $(w=1,...,V)$ [Zhuravchak, Zabrodska, 2024]. We obtain systems of linear algebraic equations (SLAE) for determining the unknowns d_{mv}:

$$\sum_{v=1}^{V} d_{0v}\int_{G_{0v}}(\mathbf{E}_{0h}(x^w,\xi,\sigma_0)+\lambda\mathbf{F}_{0h}(x^w,\xi,\sigma_0))dG_{0v}(\xi)-\sum_{v=1}^{V} d_{1v}\int_{G_{1v}}\mathbf{E}_1(x^w,\xi,\sigma_1)dG_{1v}(\xi)-C_1=$$
$$=-\int_{\Gamma_j}(\mathbf{E}_{0h}(x^w,\xi,\sigma_0)+\lambda\mathbf{F}_{0h}(x^w,\xi,\sigma_0))\psi(\xi_1,0)d\Gamma_j(\xi)\,,$$
$$x^w\in\partial\Omega_1\,, \qquad (10)$$
$$\sigma_0\sum_{v=1}^{V} d_{0v}\int_{G_{0v}}\mathbf{F}_{0h}(x^w,\xi,\sigma_0)dG_{0v}(\xi)-\sigma_1\sum_{v=1}^{V} d_{1v}\int_{G_{1v}}\mathbf{F}_1(x^w,\xi,\sigma_1)dG_{1v}(\xi)=$$
$$=-\sigma_0\int_{\Gamma_j}\mathbf{F}_{0h}(x^w,\xi,\sigma_0)\psi(\xi_1,0)d\Gamma_j(\xi)\,,\ x^w\in\partial\Omega_1\,; \qquad (11)$$

We supplement the system of equations (10), (11) with the condition of equality of zero in the sum of all sources at infinity:

$$\sum_{v=1}^{V} d_{1v}\int_{G_{1v}} dG_{1v}(\mathsf{x})+C_1=0\,. \qquad (12)$$

In the last step, we substitute the obtained solutions of the SLAE (10)-(12) d_{mv} into (8), (9).

Solving the direct problem of the theory of the potential field of the IP for the cases of volume and mixed polarization

In the case of volume polarization, the SLAE for finding the unknowns d_{mv} will have the form (we satisfy the boundary conditions (2)):

$$\sum_{v=1}^{V} d_{0v} \int_{G_{0v}} \mathbf{E}_{0h}(x^w,\xi,\sigma_0^*)dG_{0v}(\xi) - \sum_{v=1}^{V} d_{1v} \int_{G_{1v}} \mathbf{E}_1(x^w,\xi,\sigma_1^*)dG_{1v}(\xi) - C_1 =$$
$$= -\int_{\Gamma_j} \mathbf{E}_{0h}(x^w,\xi,\sigma_0^*)\psi(\xi_1,0)d\Gamma_j(\xi)\,,\ x^w \in \partial\Omega_1\,, \tag{13}$$

$$\sigma_0^* \sum_{v=1}^{V} d_{0v} \int_{G_{0v}} \mathbf{F}_{0h}(x^w,\xi,\sigma_0^*)dG_{0v}(\xi) - \sigma_1^* \sum_{v=1}^{V} d_{1v} \int_{G_{1v}} \mathbf{F}_1(x^w,\xi,\sigma_1^*)dG_{1v}(\xi) =$$
$$= -\sigma_0^* \int_{\Gamma_j} \mathbf{F}_{0h}(x^w,\xi,\sigma_0^*)\psi(\xi_1,0)d\Gamma_j(\xi)\,,\ x^w \in \partial\Omega_1\,; \tag{14}$$

and the integral representation are follows:

$$u_0(x,\sigma_0^*) = \sum_{v=1}^{V} d_{0v} \int_{G_{0v}} \mathbf{E}_{0h}(x,\xi,\sigma_0^*)dG_{0v}(\xi) + \int_{\Gamma_j} \mathbf{E}_{0h}(x,\xi,\sigma_0^*)\psi(\xi_1,0)d\Gamma_j(\xi)\,,\ x \in \Omega_0 \cup \partial\Omega_0\,,$$

$$e_0(x,\sigma_0^*) = -\sum_{v=1}^{V} d_{0v} \int_{G_{0v}} \mathbf{F}_{0h}(x,\xi,\sigma_0^*)dG_{0v}(\xi) - \int_{\Gamma_j} \mathbf{F}_{0h}(x,\xi,\sigma_0^*)\psi(\xi_1,0)d\Gamma_j(\xi)\,, \tag{15}$$

$$u_1(x,\sigma_1^*) = \sum_{v=1}^{V} d_{1v} \int_{G_{1v}} \mathbf{E}_1(x,\xi,\sigma_1^*)dG_{1v}(\xi) + C_1\,,\ x \in \Omega_1 \cup \partial\Omega_1\,,$$

$$e_1(x,\sigma_1^*) = -\sum_{v=1}^{V} d_{1v} \int_{G_{1v}} \mathbf{F}_1(x,\xi,\sigma_1^*)dG_{1v}(\xi)\,. \tag{16}$$

In the case of mixed-type polarization, we satisfy boundary conditions (3), i.e., the SLAE consists of equations similar to (10):

$$\sum_{v=1}^{V} d_{0v} \int_{G_{0v}} (\mathbf{E}_{0h}(x^w,\xi,\sigma_0^*) + \lambda\mathbf{F}_{0h}(x^w,\xi,\sigma_0^*))dG_{0v}(\xi) - \sum_{v=1}^{V} d_{1v} \int_{G_{1v}} \mathbf{E}_1(x^w,\xi,\sigma_1^*)dG_{1v}(\xi) - C_1 =$$
$$= -\int_{\Gamma_j} (\mathbf{E}_{0h}(x^w,\xi,\sigma_0^*) + \lambda\mathbf{F}_{0h}(x^w,\xi,\sigma_0^*))\psi(\xi_1,0)d\Gamma_j(\xi)\,,\ x^w \in \partial\Omega_1\,, \tag{17}$$

and the system of equations (14). We write the integral representations by formulas (15), (16).

Each of the systems of equations (13), (14) or (17), (14) is supplemented by condition (12).

Solving the inverse problem of the field potential theory of the VP

Let us assume that the separation boundary $\partial\Omega_1$ is given by a quadrilateral. The cascade iterative recognition algorithm will first be written for the case of surface polarization of the inclusion (we consider the medium to be unpolarized).

Step 1. By the nature of the change in apparent resistivity and apparent polarizability (assuming a linear dependence of the induced polarization of ionic and electronic conductors on the current density):

$$\rho_a = \frac{k_u}{I}\left|u_0^N(x_M,s_0) - u_0^N(x_N,s_0)\right|,$$

$$\eta_a = \frac{e_0^{IP}(x,s_0)}{e_0(x,s_0)} = \frac{\partial u_0^{IP}(x,s_0)}{\partial \mathbf{n}(x)} \Big/ \frac{\partial u_0^N(x,s_0)}{\partial \mathbf{n}(x)}\,, \tag{18}$$

we determine the sign and initial approximations for $\Delta s, \Delta l$, taking into account that

$$s_1 = s_{1,0} + \Delta s\,,\ l = l_0 + \Delta l\ , \tag{19}$$

initial approximations (x_{10}, x_{20}) – the center of mass of the inclusion, modeled by a rectangle with sides $2l_1$, $2l_2$, x_{10} we determine exactly by the extremum of the curve ρ_a (18) or η_a (19), x_{20} and l_1 , l_2 – approximately by this curve, integrated within the limits between its inflection points.

Here k_u is the coefficient of the installation ABMN [Zhuravchak, Zabrodska, 2024]; it is clear that the apparent resistivity and apparent polarizability of a homogeneous half-plane are equal to unity at each point.

The potential of the field IP is calculated as the difference of the potentials of the full polarized field $u_0^P(x,s_0)$ and the primary field $u_0^N(x,s_0)$:

$$u_0^{IP}(x,s_0) = u_0^P(x,s_0) - u_0^N(x,s_0)\,,$$

where $u_0^N(x,s_0)$ is obtained as a solution to the problem of potential theory (4), (7) in an unpolarized medium [Zhuravchak, Zabrodska, 2024], supplemented at the contact boundary by the conditions

of continuity of the potential and normal components of the current density:

$$u_0(x) = u_1(x),\ \sigma_0 \frac{\partial u_0(x)}{\partial \mathbf{n}(x)} = \sigma_1 \frac{\partial u_1(x)}{\partial \mathbf{n}(x)},\ x \in \partial\Omega_1,$$

$u_0^P(x,\sigma_0)$ is a solution to the problem (1), (4), (7).

Step 2. We assume that $\sigma_{1,0}$ and λ_0 are known.

Step 3. We organize the first cascade of iterations to clarify the location of the local heterogeneity and its approximate dimensions.

1. We model ∂W_1 with a rectangle with vertex coordinates:

$$x_1^1 = x_{10} - l_1, x_2^1 = x_{20} - l_2,$$
$$x_1^2 = x_{10} + l_1, x_2^2 = x_{20} - l_2,$$
$$x_1^3 = x_{10} + l_1, x_2^3 = x_{20} + l_2,$$
$$x_1^4 = x_{10} - l_1, x_2^4 = x_{20} + l_2. \quad (20)$$

2. For the selected $\sigma_{1,0}$ and λ_0 using the above-described algorithm for solving the direct problem, we calculate the potential of the IP field $u_0(x)$ by formula (8) for $x \in \partial W_b$.

3. Minimize the functionality

$$I^f = \int_{\partial W_b} |u_b(x) - u_0(x)|\, d\partial W_b(x), \quad (21)$$

allowing variation only x_{20}, l_1, l_2.

4. We fix x_{20}^f, l_1^f, l_2^f, which correspond to the found minimum of the functional (21) and refine σ_1 and λ by formulas (20), using minimization (21), denote them by σ_1^f, λ^f.

5. As a result, we find, using formulas similar to (20), the refined coordinates of the vertices of the rectangle (x_1^{nf}, x_2^{nf}), n=1,…,4.

Step 4. We organize a second cascade of iterations to refine the shape and orientation in the inclusion space.

1. We will rotate the rectangle found in step 3 around its center of mass, simultaneously scaling along the axes. To do this, we introduce three new parameters φ_0, s_1, s_2 and calculate new coordinates of the vertices of the rectangle:

$$x_1^{nr} = (x_1^{nf} - x_{10})\cos\varphi_0 - (x_2^{nf} - x_{20}^f)\sin\varphi_0 + x_{10},$$
$$x_2^{nr} = (x_1^{nf} - x_{10})\sin\varphi_0 + (x_2^{nf} - x_{20}^f)\cos\varphi_0 + x_{20}^f,$$
$$x_1^{nc} = x_1^{nr} s_1 + (1 - s_1)x_{10},$$
$$x_2^{nc} = x_2^{nr} s_2 + (1 - s_2)x_{20}^f. \quad (22)$$

2. We minimize the functional (21) by variation φ_0, s_1, s_2 and fix $\varphi_0^f, s_1^f, s_2^f$, which correspond to the found minimum.

3. For constants x_{10}, x_{20}^f, l_0^f (or, l_1^f, l_2^f), $\varphi_0^f, s_1^f, s_2^f$ we specify σ_1^f, λ^f using minimization (21), and denote them by $\sigma_1^{f2}, \lambda^{f2}$.

Step 5. The found ones x_1^{nc}, x_{2n}^{nc} serve instead of variables x_1^{nf}, x_2^{nf}, in formulas (22) for further refinement in the iterative process of minimization (21) with constants $\sigma_1^{f2}, \lambda^{f2}$. Note that the last two steps are sometimes advisable to repeat several times.

For the case of volume polarization of the inclusion, the cascade iterative recognition algorithm is similar to the one given above, except that now we find, in addition to geometric parameters, physical characteristics σ_1 and $\eta_1 = \eta_{1,0} + \Delta\eta$ (instead of λ), and instead of formula (19), we use this one:

$$\eta_a = \frac{e_0^{IP}(x,\sigma_0^*)}{e_0(x,\sigma_0^*)} = \frac{\partial u_0^{IP}(x,\sigma_0^*)}{\partial \mathbf{n}(x)} \Big/ \frac{\partial u_0^N(x,\sigma_0^*)}{\partial \mathbf{n}(x)},$$

and the potential of the IP field is calculated as the difference in potentials of the full polarized field $u_0^P(x,\sigma_0^*)$ and the primary field $u_0^N(x,\sigma_0)$:

$$u_0^{IP}(x,\sigma_0^*) = u_0^P(x,\sigma_0^*) - u_0^N(x,\sigma_0), \quad (23)$$

where $u_0^P(x,\sigma_0^*)$ as a solution to the problem (2), (5), (7).

The case of mixed polarization does not cause any fundamental difficulties, however, the number of physical characteristics increases to three (σ_1, λ and η_1), and $u_0^P(x,\sigma_0^*)$ in formula (23) is the solution to problem (3), (5), (7).

The results

The direct and inverse problems of direct current electrical exploration for polarized media using electrical profiling were solved by the indirect boundary element method for A=(-25, 0) and B=(25,0), and respectively. The current strength I and the electrical conductivity σ_0 of the geological medium W_0 were set equal to unity. The distance between the receiving electrodes was chosen MN = 0.1AB, and they were moved along the line (-25, 25) with a step of 0.1.

First, a volume polarized inclusion in the form of a rectangle with sides $2l_1$ =4, $2l_2$ =2, with different coefficients of induced polarization η_1 in an unpolarized medium was considered. The “center of mass” of the inclusion, i.e., the intersection point of the diagonals of the rectangle, was located at the point (0, -3), the distance from the half-plane boundary h = 2. The medium and inclusion resistivity (quantities inversely proportional to their electrical conductivities) were chosen as follows:

$$\rho_0 = 1, \rho_1 = 0.5 \text{ and } \rho_1 = 2.$$

We investigated the change in the shape of the apparent resistivity ρ_a and apparent polarizability η_a curves calculated over the inclusion when the coefficient was changed η_1 for cases where the inclusion resistivity was less (Fig. 1, *a*) and greater (Fig. 1, *b*) than the resistivity of the medium. Only the apparent resistivity graphs are presented, since the apparent polarizability graphs had a similar appearance.

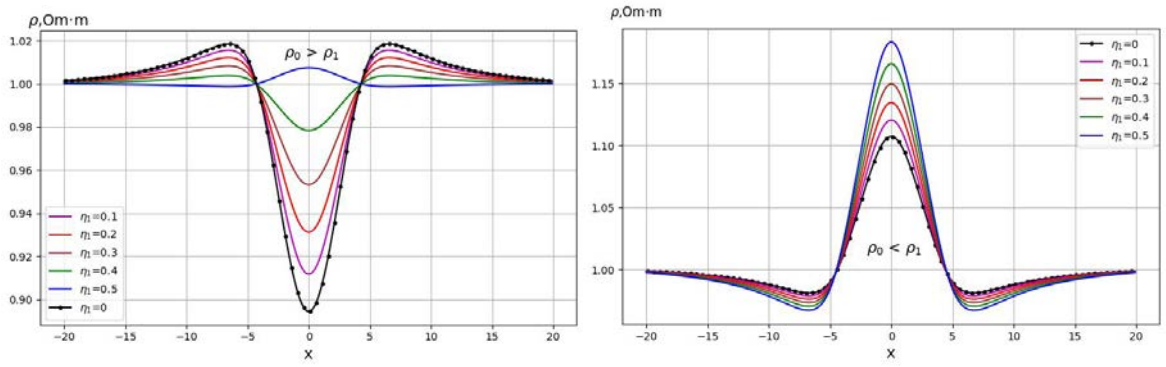

a *b*

Fig. 1. Graphs of apparent resistivity over a volume polarized inclusion at different induced polarizability coefficients for cases when the inclusion resistivity is less (a) and greater (b) than the resistivity of the medium.

As we can see, each graph is characterized by three extrema: the central one and two symmetrical ones with respect to it. The central extrema can be used to estimate the magnitude of the inclusion resistivity (whether it is greater or less than the resistivity of the medium) and to determine the coordinate x_1 of the "center of mass" of the inclusion, and the horizontal distance between the symmetrical extrema – the horizontal dimensions of the inclusion. The value of the induced polarization coefficient η_1 for such graphs will be determined taking into account the difference between the extrema of the curves corresponding to polarized and non-polarized inclusions, since an increase η_1 leads to a decrease in the magnitude of the extrema in case (a) and to its increase in case (b).

The acquired graphs resemble the apparent resistivity graphs calculated for various depths h and different electrical conductivity values of the inclusion, excluding polarizability. However, there is no complete overlap between them. This observation indicates that each unique set of characteristics for the studied region corresponds to a specific distribution of apparent resistivity.

Next, the cases of surface polarization (with different values of the coefficient at the boundary of the inclusion) and mixed polarization (Fig. 2, *a*) are considered. As can be seen from Fig. 2, *a*, an increase in the coefficient of surface polarization is reflected in a decrease in the value of the central extremum on the graphs. From the graphs (Fig. 2, *b*), it is clear that the greatest influence is observed with volume polarization; therefore, when solving the inverse problem, we will consider this particular case. Surface polarization has a much smaller influence, but it is significantly enhanced in the case of mixed polarization.

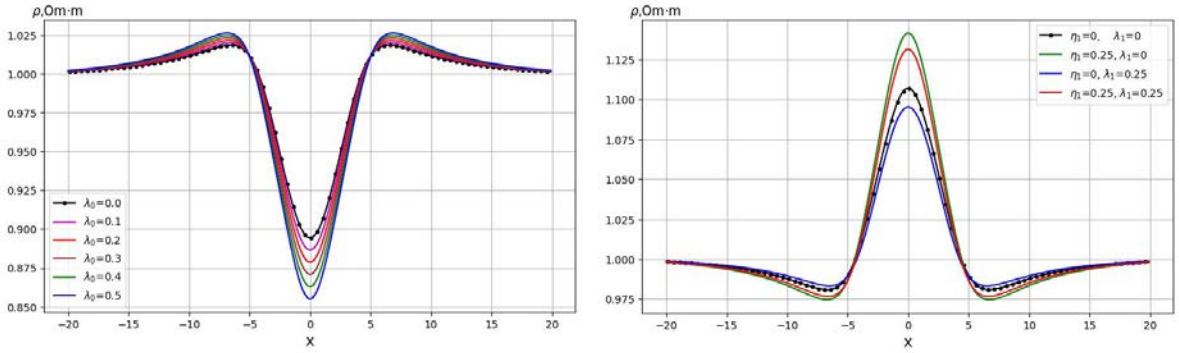

a *b*

Fig. 2. Graphs of apparent resistivity over an inclusion with surface (a) and mixed (b) polarizationfor cases when the inclusion resistivity is less (a) and greater (b) than the resistivity of the medium.

The graphs shown in Fig. 1 a nd 2 are used to select initial approximations for the geometric and physical characteristics of the inclusion. In particular, the convexity in the graphs in Fig. 1 indicates that the resistivity of a polarized inclusion is greater than the resistivity of an unpolarized medium, so we set $\Delta\sigma, \Delta\sigma^*$ to be negative. The coordinate x_{10} is determined exactly by the extremum of the curve ρ_a, and x_{20} and l_1, l_2 are approximately by this curve, integrated within the limits between its inflection points. The horizontal size of the inclusion l_1 will be less than the distance between the minima of the curve by approximately 50 %, and the vertical size l_2 and depth of the center of mass h will be proportional to the height of the maximum on the graph.

The inverse problem for inclusion in the form of a rectangle with sides $2l_1 = 4$, $2l_2 = 2$, placed horizontally (i. e., with its longer side parallel to the day surface), is solved for the case of volumetric polarization. Having found the initial approximations, the values of the functional are calculated for two fixed parameters ($\sigma_{1,0} = 0.5$ and $h = 2$) and two variables (the sides of the rectangle). We find the range of values of the variable parameters in the vicinity of which the functional is minimal. Fig. 3 presents contour lines that show that there are areas where the values of the functional are the smallest, and they cover possible pairs of solutions to the problem: the desired values l_1 are in the range from 1 to 2.1, and l_2 from 0.2 to 2, which is displayed in the figures by a wider light strip.

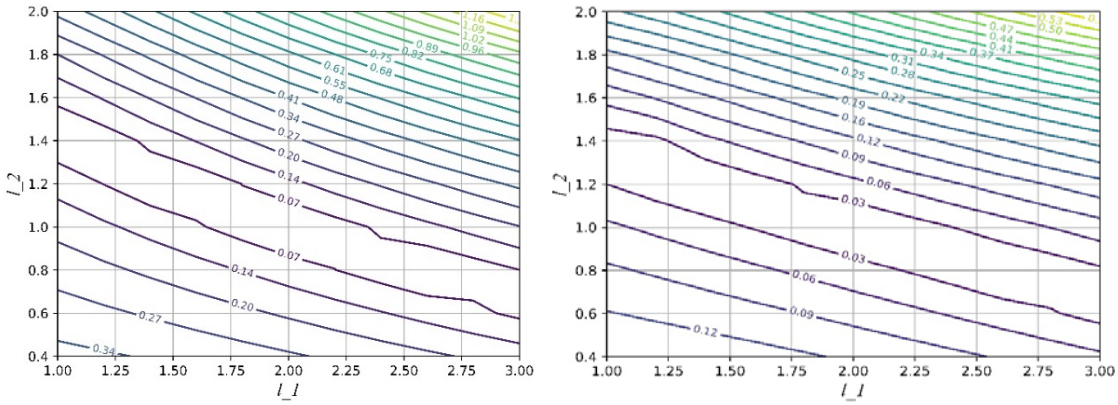

Fig. 3. Isoline graphs of the values of the functional calculated with two fixed parameters (a – $\sigma_1 = 0.5$, $h = 2$) and two variables (sides of the rectangle) for a polarized inclusion (a) and the values of the modulus of the difference of the functionals for polarized and unpolarized inclusions (b).

It should be noted that the difference between the values of the functionals corresponding to polarized and non-polarized inclusions makes it possible to estimate the induced polarization coefficient. The proposed approaches have been implemented in software using the modern and powerful Python programming language, as it is free to use and offers a large number of additional libraries, such as NumPy, SciPy, Matplotlib, and others. The use of these libraries significantly accelerates and simplifies the development of programs, enabling visual control over the processes of constructing the geometric research domain, the discrete model, and the overall computational procedure.

A volume-polarized inclusion in the form of a rhombus was also considered to test the 4th and 5th steps of the algorithm and the case of surface polarization for a rectangle; these results are not presented because they did not cause fundamental differences in implementation.

Based on the proposed approach, automated computer modules were developed in Python to solve the direct and inverse problems of the potential theory of induced polarization.

In future research, we plan to extend the proposed algorithm for solving the inverse problem using profiling for two, three, or more horizontally arranged inclusions with identical or different electrical conductivities. We also aim to develop an algorithm for detecting two vertically aligned inclusions using the method of vertical electrical sounding.

Originality

Using mathematical modeling, the problem of DC geoelectrical surveying in piecewise homogeneous polarized media has been reduced to potential theory problems with imperfect contact conditions at the interfaces between different media.

Practical significance

An efficient computational approach has been developed for solving the inverse problem of DC electrical sounding, which accounts for the effect of induced polarization in cases of surface, volume, and mixed polarization. Time optimization is achieved through a two-stage cascade-iterative algorithm that refines initial approximations and eliminates parameters with negligible influence on the result.

Conclusions

1. The calculation of induced polarization (IP) fields is reduced to determining the polarized field within the medium, followed by computing the difference between the polarized and primary fields. The polarized field is defined as the total field acting during the charging period, while the primary field refers to the initial current field at the moment of charging onset, when IP effects can be neglected. At any fixed moment during charging, the polarized field satisfies Laplace's equation. It is computed using the same methods as for the direct current field, under identical boundary conditions. However, the contact conditions are more complex and vary depending on whether the induced polarization is of surface, volume, or mixed type.Induced polarization (the formation of surface and volume charges in the rock) can occur only in multi-component media consisting of a solid matrix and an electrolyte fluid. IP effects are particularly pronounced in areas with disseminated sulfide mineralization and graphitized geological formations and ion-conductive rocks. The electric field of a point source in a polarized medium is described by the same relations as in a non-polarized medium, except that the resistivity of the polarized medium ρ^* replaces the standard resistivity ρ. The manifestation of induced polarization is characterized by frequency-dependent dispersion of electrical resistivity, which leads to a phase shift between the power source's current and the voltage measured in the polarized medium.

2. The proposed methodology makes it possible:

– to solve the direct problem and determine the potential of the IP field in a piecewise-homogeneous half-space with an inclusion of arbitrary shape;

– to place point and finite-sized sources of various types, as well as observation points, anywhere within the half-space, simulating both surface and borehole measurements;

– to solve the inverse DC resistivity problem, taking into account cases of surface, volume, and mixed types of induced polarization.

3. The developed methods of research and consideration of the effect of induced polarization (IP) make it possible to investigate the distribution of the potential field in heterogeneous media. By examining the the spatial distribution of the calculated apparent resistivity and polarization, to identify fluid zones, faults, boundaries of tectonic blocks, as well as zones of metasomatism − processes directly related to geodynamic changes in the lithosphere. This analysis is particularly important for regions with seismotectonic activity.

4. The obtained results can also be applied to developing recognition methods in exploration geophysics for delineating mineral deposits. Additionally, they can be utilizedin materials science and defectoscopy for determining the location and dimensions of foreign inclusions and defects.

References

Alfouzan, F., Alotaibi, A., Cox, L., & Zhdanov, M. S. (2020). Spectral Induced Polarization Survey with Distributed Array System for Mineral Exploration: Case Study in Saudi Arabia. *Minerals*, 10, 769. https://doi.org/10.3390/min10090769

Bérubé, Charles L., & Gagnon, Jean-Luc. (2025). Anisotropic induced polarization modeling with neural networks and effective medium theory. *Geophysics,* 90, 2. https://doi.org/10.1190/geo2024-0107.1

Bérubé, Charles, L., & Bérubé, Pierre. (2022). Data-driven modeling of time-domain induced polarization. *Geophysics*, 87, 3. https://doi.org/10.1190/geo2021-0497.1

Brusak, I., Maciuk, K., & Haidus, O. (2025). Detection of geodynamic anomalies in GNSS time series using machine learning methods. *Geodynamics,* 1(38): 37−48. https://doi.org/10.23939/jgd2025.01.037

Caowei, Wu, Changchun, Zou, Cheng, Peng, Yang, Liu, Tao, Wu, Jianping, Zhou, & Chunhui, Tao. (2022). Numerical Simulation Study on the Relationships between Mineralized Structures and Induced Polarization Properties of Seafloor Polymetallic Sulfide Rocks. *Minerals*, 12(9), 1172. https://doi.org/10.3390/min12091172

Cox, Leif H., Zhdanov, Michael S., Pitcher, Douglas H., & Niemi, Jeremy. (2023). Three-Dimensional Inversion of Induced Polarization Effects in Airborne Time Domain Electromagnetic Data Using the GEMTIP Model. *Minerals*,·13(6): 779. https://doi.org/10.3390/min13060779

Davies, L., Ley-Cooper, A. Y., Sutton, M., & Drovandi, C. (2023). Bayesian detectability of induced polarization in airborne electromagnetic data. *Geophysical Journal International*, 235, 3, Pages 2499–2523. https://doi.org/10.1093/gji/ggad073

Finden, Erlend, Skartlien, Roar, Holm, Sverre, & Hamran, Svein-Erik. (2024). Induced polarization in the transient electromagnetic method for detection of subsurface ice on Earth, Mars, and the Moon. *Planetary and Space Science,* 254. https://doi.org/10.1016/j.pss.2024.106007

Fys, M., Brydun, A., & Vovk, A. (2023). Algorithm for constructing the subsoil density distribution function considering its value on the surface. *Geodynamics,* 2(35): 72−79. https://doi.org/10.23939/jgd2023.02.072

Hongzhu, Cai, & Zhdanov, Michael S. (2017). Finite-element time-domain electromagnetic modeling with induced-polarization effects using adaptive Padé. *SEG International Exposition and Annual Meetingseries*. https://doi.org/10.1190/segam2017-17795904.1

Jiaxuan, Ling, Wei, Deng, Shiwei, Wei, Qingrui, Chen, Lihua, He, Siqin, Liu, & Mengmeng, Li. (2024). Research on 3D modelling of induced polarization in polarizability anisotropic media. *Geophysical Prospecting*, 72(5). https://doi.org/10.1111/1365-2478.13580

Kamran, M., & Hamidreza, R. (2019). Investigating the applicability of induced polarization method in ore modelling and drilling optimization: a case study from Abassabad, Iran Near Surface, *Geophysics*, 17, 6. https://doi.org/10.1002/nsg.12055

Pourhashemi, Seyyed Sajjad, Ghanati, Reza, & Aliheidari, Ashkan. (2024). Time-Domain Induced Polarization Tomography Inversion. *International Journal of Mining and Geo-Engineering*, 58, 2. DOI*:* 10.22059/IJMGE.2024.367235.595113

Revil, A. & Gresse, M. (2021**)**. Induced polarization as a tool to assess alteration in geothermal systems: a review. *Minerals,* 11, 962. https://doi.org/10.3390/min11090962

Revil, A., Qi, Y., Ghorbani, A., Gresse, M., & Thomas, D. M. (2021**)**. Induced polarization of volcanic rocks. 5. Imaging the temperature field of shield volcanoes. *Geophysical Journal International*, 225, 3, 1492–1509. https://doi.org/10.1093/gji/ggab039

Satoshi, Izumoto. (2023). Induced Polarization of Metal Grains: Simulations of Three-Dimensional Electric Fields. *Journal of Geophysical Research: Solid Earth,* 128(9). https://doi.org/10.1029/2023JB026757

Yanju, Ji, Xiangdong, Meng, Weimin, Huang, Yanqi, Wu, & Gang, Li. (2020). 3D Numerical Modeling of Induced-Polarization Grounded Electrical-Source Airborne Transient Electromagnetic Response Based on the Fictitious Wave Field Methods. *Appl. Sci.* https://doi.org/10.3390/app10031027

Yanju, Ji, Yanqi, Wu, Shanshan, Guan, & Xuejiao, Zhao (2018). 3D numerical modeling of induced-polarization electromagnetic response based on the finite-difference time-domain method. *Geophysics*, 83(6), E385–E398. https://doi.org/10.1190/geo2017-0190.1

Ye, Yx., Li, Yg., Deng, Jz. *et al.* (2014) 2.5D induced polarization forward modeling using the adaptive finite-element method. *Appl. Geophys.* 11, 500–507. https://doi.org/10.1007/s11770-014-0455-z

Zhdanov, M. (2008). Generalized effective-medium theory of induced polarization. *Geophysics*, 73, F197–F211. https://doi.org/10.1190/1.2973462

Zhuravchak, L. (2019). Mathematical Modelling of Non-stationary processes in the Piecewise-Homogeneous Domains by N ear-Boundary Element Method. *Advances in Intelligent Systems and Computing*, 1080 AISC, 64–77, N. Shakhovska and M. O. Medykovskyy (Eds.). https://doi.-org/10.1007/978-3-030-33695-0_6

Zhuravchak, L. M. (2024). Potential field modeling by combination of near-boundary and contact elements with non-classical finite differences in a heterogeneous medium. *Mathematical Modeling and Computing*, 11, 2, 373–384. https://doi.org/10.23939/mmc2024.02.373

Zhuravchak, L. M., & Kruk, O. S. (2015). Consideration of the nonlinear behavior of environmental material and a three-dimensional internal heat sources in mathematical modeling of heat conduction. *Mathematical Modeling and Computing*, 2, 1, 107–113. https://doi.org/10.23939/mmc2015.01.107

Zhuravchak, L., & Zabrodska, N. (2024). Algorithm for determining inclusion parameters in solving inverse problems of geoelectrical exploration using the profiling method. *Geodynamics,* 1(36): 98–107. https://doi.org/10.23939/jgd2024.01.098

Zhuravchak, L.M., & Zabrodska, N.V. (2010). Nonstationary thermal fields in inhomogeneous materials with nonlinear behavior of the components. *Materials Science*, 46 (1), 36–46. https://doi.org/10.1007/s11003-010-9261-9

Zibulski, E., & Klitzsch, N. (2023). Influence of Inner Surface Roughness on the Spectral Induced Polarization Response – A Numerical Study. *Journal of Geophysical Research: Solid Earth*, 127, 10. https://doi.org/10.1029/2022JB025548

Любов ЖУРАВЧАК[1], Наталія ЗАБРОДСЬКА[2]

[1] Національний університет “Львівська політехніка”, вул. С. Бандери, 12, Львів, 79013, Україна, тел. +38(032)2582578, ел. пошта: liubov.m.zhuravchak@lpnu.ua, https://orcid.org/ 0000-0002-1444-5882
[2] Карпатське відділення Інституту геофізики ім. С. І. Субботіна НАН України, вул. Наукова, 3-б, м. Львів, 79060, Україна, тел. +38(032)2648563, ел. пошта: nataliya.zabrodska@gmail.com, https://orcid.org/ 0009-0001-8850-6721

ВРАХУВАННЯ ЕФЕКТУ ВИКЛИКАНОЇ ПОЛЯРИЗАЦІЇ ПІД ЧАС РОЗВ’ЯЗУВАННЯ ОБЕРНЕНИХ ЗАДАЧ ГЕОЕЛЕКТРИЧНИХ ЗОНДУВАНЬ

Мета роботи – з використанням непрямого методу пригранічних елементів побудувати алгоритм розпізнавання фізичних (поляризовності й питомого електричного опору) та геометричних (центра мас, орієнтації та розмірів) характеристик локальної неоднорідності за даними потенціалу поля викликаної поляризації (ВП), виміряного на межі об’єкта. Методика. За модель земної кори вибрано кусково-однорідну півплощину, складові якої перебувають у неідеальному контакті. Для розв’язування оберненої двовимірної задачі теорії потенціалу поля ВП розроблено ефективне поєднання непрямого методу пригранічних елементів із каскадним ітераційним алгоритмом розпізнавання характеристик. На кожному кроці алгоритму розв’язано низку прямих задач, в яких здійснено перехід від системи рівнянь Лапласа до інтегральних подань з функцією Гріна для півплощини (вона автоматично задовольняє крайову умову і дає змогу уникнути дискретизації її межі) та фундаментальним розв’язком для включення. Умови неідеального контакту задоволено в колокаційному сенсі у середині кожного граничного елемента, що дало можливість знайти інтенсивності невідомих джерел, уведених у пригранічних елементах і апроксимованих сталими. Після цього середовище і включення розглянуто як цілком незалежні ділянки, в них обчислено шуканий потенціал поля ВП та потік через їхні межі. Результати. Обчислювальний експеримент виконано для задачі електророзвідки постійним штучним полем методом ВП (електропрофілюванням). За змінами позірного опору та позірної поляризовності визначено початкові наближення для фізичних та геометричних характеристик включення. За допомогою організованих двох каскадів ітерацій спочатку уточнено його місцезнаходження та приблизні розміри, а потім – форму та орієнтацію у просторі. Необхідною умовою успішного розпізнавання є наявність ділянки межі із заданим надлишком крайових умов, що дало змогу виконати мінімізацію розглянутого на ній функціоналу. Наукова новизна. За допомогою математичного моделювання задачі геоелектророзвідки постійним струмом у кусково-однорідних поляризованих середовищах зведено до задач теорії потенціалу з умовами неідеального контакту на межах поділу середовищ. Практична значущість. Розроблено ефективний обчислювальний підхід до розв’язування оберненої задачі електророзвідки постійним струмом, який враховує вплив ефекту викликаної поляризації для випадків поверхневої, об’ємної та змішаної поляризації. Часової оптимізації досягнуто за рахунок двоетапності каскадного ітераційного алгоритму для уточнення початкових наближень та відкидання параметрів, що мало впливають на результат.

Ключові слова: математичне моделювання, викликана поляризація, пряма задача, обернена задача, непрямий метод пригранічних елементів, кусково-однорідне поляризоване середовище, електричне профілювання.

Received 14.07. 2025